Depicting the roles of CuO secondary phase and heat treatment in driving the magnetic and magnetocaloric features of $Pr_{2/3}Sr_{1/3}MnO_3$ manganite

O. Chdil, M. Balli, N. Brahiti, R. Essehli, Patricia de Rango, P. Fournier, S. Naamane, K. El Maalam, O. Mounkachi

Depicting the roles of CuO secondary phase and heat treatment in driving the magnetic and magnetocaloric features of $Pr_{2/3}Sr_{1/3}MnO_3$ manganite

O. Chdil[a,*], M. Balli[a,b,*], N. Brahiti[b], R. Essehli[c], P. de Rango[d], P. Fournier[b], S. Naamane[e], K. El Maalam[e], O. Mounkachi[f,g]

[a]*AMEEC team, LERMA, College of Engineering and Architecture, International University of Rabat, parc Technopolis, Rocade de Rabat-Salé, 11100, Morocco*
[b]*Institut quantique, Département de Physique and RQMP, Université de Sherbrooke, Sherbrooke, Québec, Canada J1K 2R1*
[c]*Energy and Transportation Science Division, Oak Ridge National Laboratory, Oak Ridge, TN, 37830, USA*
[d]*Université Grenoble Alpes, CNRS, Institut Néel, 38000 Grenoble, France*
[e]*Durability and Engineering of Materials Center, Moroccan Foundation for Advance Science Innovation and Research (MAScIR), Rabat, Morocco*
[f]*Laboratory of Condensed Matter and Interdisciplinary Sciences (LaMCScI), Faculty of Sciences, Mohammed V University in Rabat, Morocco*
[g]*MSDA, Mohammed VI Polytechnic University, Lot 660, Hay Moulay Rachid Ben Guerir, 43150, Morocco*

Abstract

In this work, we report a detailed experimental study regarding the impact of copper oxide (CuO) secondary phase and heat treatments on the structural, magnetic, and magnetocaloric properties of the near-room temperature $Pr_{2/3}Sr_{1/3}MnO_3$ (PSMO) magnetic refrigerant. Our investigations are carried out by using structural and microstructural analyses, alongside magnetization measurements. The analysis of X-ray diffraction data of PSMO(95%)-CuO(5%) (PSMO-CuO) samples shows the coexistence of both CuO and PSMO phases. Further, the microstructural analysis of PSMO-CuO reveals that the addition of CuO significantly enhances the grains size. On the other hand, the added secondary phase markedly reduces the Curie temperature (T_c) from 293 K for PSMO to about 273 K for PSMO-CuO composite while increasing the magnetocaloric effect. This decrease in T_c is associated with a significant change from 162° to about 156° in the Mn-O_{II}-Mn bond angle respectively. Moreover, performed investigations regarding the role of heat treatments unveil that the observed changes in the structural and magnetic features are mainly driven by the secondary phase that modify grains size and double-exchange interactions in the PSMO compound. Interestingly, our findings demonstrate that the Curie temperature of the PSMO and accordingly its magnetocaloric effect can be tailored by adding small amounts of CuO without need to substitution on cation sites. In the light of obtained results, a multilayered refrigerant composed of PSMO and PSMO-CuO is proposed to cover the magnetic cooling temperature range close to room-temperature. The resulting entropy change remains practically constant between 273 K and 293 K. Such a behavior is highly appreciated from a practical point of view, particularly in cases where the cooling process is carried out by using the AMR and Ericsson cycles.

Keywords: Magnetocaloric effect, Manganites composites, Secondary phase, Heat treatment, Grains size

1. Introduction

Near-room temperature solid-state magnetic refrigeration is a new and rapidly growing area of materials science and engineering [1–6], due to its high thermal efficiency and the absence of air pollutants. This makes magnetic refrigeration a serious alternative to conventional techniques [7, 8]. Currently, there are several prototype devices worldwide that use the magnetocaloric effect to generate higher temperature spans and cooling powers [9, 10]. However, there is currently no mass-market product available for purchase [11]. This is because various hurdles must be overcome before magnetic refrigeration can be commercialized, such as corrosion and mechanical brittleness issues, as well as the discovery of a magnetocaloric material with large MCE over a wide temperature range combined with low hysteresis, low cost, and high electrical resistance. Magnetic refrigeration is based on the magnetocaloric effect (MCE) of magnetic materials, which are used to create a regenerator matrix representing the heart of magnetocaloric systems [12–14]. The MCE is defined as the change in temperature (magnetic entropy) of a magnetic material when it is adiabatically exposed to an external magnetic field (isothermally) [15]. The atomic and spin latices are the two major contributors to the overall change in entropy. Under the influence of an external magnetic field, the coupling between atomic and magnetic lattices, in typical ferromagnets and paramagnets, results in the material cooling (heating) when the magnetic moments are disordered (ordered) [16]. An effective refrigerant material must have a higher ΔS_m and ΔT_{ad} values, high thermal conductivity, and low specific heat capacity [17, 18]. Various families of materials were implemented in magnetic cooling, including gadolinium, rare earth alloys, and intermetallics [19–24]. Unfortunately, the majority of these materials exhibit chemical instabilities (corrosion and oxidation) in aqueous environments, being harmful to active magnetic refrigerators (AMR) [12, 13, 15]. Additionally, most of the reported MCE materials include costly components or require complicated and expensive production processes [14, 19, 25].

*Corresponding author.
Email addresses: oumayma.chdil@uir.ac.ma (O. Chdil), mohamed.balli@uir.ac.ma (M. Balli)

In this context, the mixed-valence manganese perovskites, with the chemical formula $R_{1-x}A_xMnO_3$, in which R is a rare-earth cation (Pr^{3+}, La^{3+}, Nd^{3+}, Y^{3+}) and A an alkali or alkaline earth cation (Sr^{2+}, Ca^{2+}, Ba^{2+}, K^+, Na^+), have recently attracted the interest of researchers due to their significant magnetocaloric effects near ambient temperature and the possibility of tailoring their magnetocaloric properties because of the strong coupling between their spin, charge, orbital, and lattice degrees of freedom [26–28]. Furthermore, they are also suitable for magnetic refrigeration applications owing to their relatively low cost, easy preparation, increased chemical stability, reduced magnetic hysteresis, and low eddy current heating [29]. Manganites with mixed-valence states may be considered as a solid solution combining end members like $La^{3+}Mn^{3+}O_3^{2-}$ and $Ca^{2+}Mn^{4+}O_3^{2-}$, resulting in mixed-valence $La^{3+}_{1-x}Ca^{2+}_xMn^{3+}_{1-x}Mn^{4+}_xO_3^{2-}$ compounds [30, 31]. Typically, end members are antiferromagnetic and insulating, but solid solutions with $x = 1/3$ are ferromagnets and conductors [32]. Therefore, the specific composition, $R_{2/3}A_{1/3}MnO_3$, is attractive for magnetic refrigeration, since a ratio of Mn^{4+}/Mn^{3+} equal to 0.5 allows combining large magnetization and high Curie temperature [33]. Moreover, the MnO_6 octahedral environment in manganites may be altered chemically by substituting A- or Mn-sites, which primarily affects the charge density and produce lattice distortions. The doping of A^{2+} site with divalent ions leads to mixed-valence manganite systems in which ferromagnetic (FM) double exchange (DE) Mn^{3+}-O^{2-}-Mn^{4+} competes with antiferromagnetic (AFM) super-exchange Mn^{3+}-O^{2-}-Mn^{3+} [34–37]. The magnetic and magnetocaloric properties of these materials are highly dependent on the strength of DE interactions between Mn^{3+}/Mn^{4+} ions, which are caused by the e_g electrons migration between two partly filled d-orbitals [38]. Moreover, the discrepancy in the average ionic radii of A-site cations results in variations in the Mn-O-Mn bond angles and Mn-O bond lengths, leading to the octahedral tilting of MnO_6 [39–44]. In contrast to the A-site substitution, the replacement of a transition metal ion at the Mn site may result in altered magnetic interactions between Mn and the replaced ion, transforming then the magnetic order from FM to an AFM state or conversely [45–48].

Numerous techniques have been proposed with the aim of tailoring the magnetocaloric effect of $R_{1-x}A_xMnO_3$ manganite oxides, including hydrostatic pressure [49–51], doping with other rare earth elements [52, 53], and the insertion of secondary phases [54–61]. In fact, both the structural temperature transition and the Curie temperature (T_c) increase linearly upon increasing the applied hydrostatic pressure [49]. Moreover, as revealed by Sethupathi et al. [62], the increase of praseodymium (Pr) content in $Pr_{1-x}Sr_xMnO_3$ decreases only the material Curie temperature, whereas the magnetocaloric properties remain almost unchanged. Apart from chemical replacement and hydrostatic pressure, nanoscale particle size reduction has been utilized to modify the physical characteristics of manganites [63, 64]. Additionally, the strain effect has also been shown to be an efficient approach for enhancing the magnetocaloric characteristics of oxides [65]. On the other hand, inserting a secondary phase into the manganite-based materials has been extensively investigated, initially for the purpose of improving low-field magnetoresistance (LFMR) characteristics [66–68]. The reported studies demonstrate that incorporation of an insulating secondary phase into the manganite materials is an efficient method for creating phase boundaries and accordingly generating a colossal low-field magnetoresistance [69–72]. On the other hand, these findings have motivated researchers to investigate the impact of adding secondary phases to the manganite matrix aiming to tailor and/or enhance the magnetocaloric properties. In the reported work by El Maalam et al. [73], it was shown that the mixture of $La_{0.45}Nd_{0.25}Sr_{0.3}MnO_3$ with a small amount of CuO (typically 5% weight ratio) induces a slight decrease in the Curie temperature and enhances the magnetocaloric effect, which is, according to the authors, attributed to the larger grain size. Bhatt et al. [74] have also investigated the effect of adding Ag_2O to the pristine $Pr_{2/3}Sr_{1/3}MnO_3$ oxide, where it has been demonstrated that the magnetic entropy change exhibits surprisingly a rising trend as Ag_2O concentration increases without affecting T_c. Recently, Neupane et al. [75] reported a study in which they discussed the influence of NiO, CuO, and CoO transition metal oxides on the nanomaterial $La_{0.45}Nd_{0.25}Sr_{0.3}MnO_3$ magnetocaloric effect. Their research work demonstrates the possibility of a potential nanocomposite with increased magnetocaloric characteristics. Especially, it was demonstrated that the $La_{0.45}Nd_{0.25}Sr_{0.3}MnO_3$ - 2.5 Wt. % CuO nanocomposite displays $\Delta S_m \simeq -3.95$ J kg^{-1} K^{-1} under a magnetic field of 5 T, which is 110% higher than its equivalent of pristine material. This is associated with the increase of T_c from 240 K (pristine) to 284 K (composite). However, the driving mechanisms behind such marked changes regarding T_c and the magnetic entropy changes are not clearly explained. In addition, Neupane et al. [75] findings are in full contradiction with El Maalam et al. [73] results.

From a practical point of view, the $Pr_{1-x}Sr_xMnO_3$ series are one of the most interesting perovskites for magnetic refrigeration due to their large magnetization near to the ambient temperature and their strong chemical resistance that compensates for their relatively moderate magnetocaloric effect [76, 77]. Additionally, the substitution approach can be used to modify the Curie temperature, with a change of about 4 K in T_c per percent (%) of Sr [78, 79]. In the performed study by Repaka et al. [80], the magnetization and the magnetocaloric effect of the polycrystalline $Pr_{0.6}Sr_{0.4}MnO_3$ were particularly investigated. It was observed that the studied compound shows a second-order FM to paramagnetic (PM) transition at T_c = 305 K, with a magnetic entropy change of 2.185 J kg^{-1} K^{-1} and 3.416 J kg^{-1} K^{-1} for a field change of 1.5 T and 3 T, respectively. Furthermore, Chanda et al. [81] have demonstrated that for the same composition ($Pr_{0.6}Sr_{0.4}MnO_3$), a structural transition from the orthorhombic to the monoclinic phase occurs at T_s = 86 K. The latter significantly increases under the application of hydrostatic pressure to reach 113 K, while the Curie temperature remains almost unchanged. On the other hand, Guillou et al. [33] have reported an experimental study on

$Pr_{0.66}Sr_{0.34}MnO_3$ synthesized by the solid-state reaction method followed by a pelletization process. Particularly, it was shown that the $Pr_{0.66}Sr_{0.34}MnO_3$ compound exhibits an FM-PM transition at T_c = 295 K. Moreover, under a magnetic field change of 1 T, a magnetic entropy variation and an adiabatic temperature change of 2.3 J kg^{-1} K^{-1} and 1.1 K can be reached respectively. Furthermore, the implementation of $Pr_{0.66}Sr_{0.34}MnO_3$ in a reciprocating AMR-magnetic cooling device enables to generate a temperature span of roughly 5 K under a magnetic field of 1 T [33]. On the other hand, we have recently reported a detailed numerical study regarding the real potential of $Pr_{0.6}Sr_{0.4}MnO_3$ in magnetic cooling. The obtained results have unveiled the high performance of this material particularly when fully taking advantage of its MCE. Furthermore, even though the $Pr_{0.6}Sr_{0.4}MnO_3$ exhibits a relatively low magnetocaloric effect at practical fields of 1 T to 2 T, the coefficient of performance can be increased by a factor of two provided that magnetic forces are balanced in magnetocaloric devices [82].

Herein, the role of CuO and additional heat treatments (HT) in tailoring the structural, magnetic, and magnetocaloric properties of the near $Pr_{2/3}Sr_{1/3}MnO_3$ is deeply investigated. Keeping in mind the fact that previous studies did not provide a satisfactory explanation on how the secondary phases impact the magnetism and MCEs of manganites [57, 73–75]. In this way it is worthy to note that CuO oxide is a semiconductor with a narrow bandgap (E_g) of 1.2 eV [83] and an antiferromagnetic order taking place at the Neel temperature T_N = 230 K [84]. It crystallizes in the monoclinic structure with the lattice parameters of a = 4.6837 Å, b = 3.4226 Å, and c = 5.1288 Å, and β = 99.54 [85]. As a first step in our work, the PSMO (95%)-CuO (5%) (PSMO-CuO) composites were prepared via solid-state reaction. The lattice parameters, the interatomic distances, as well as the bond angles were determined by refining the X-ray diffraction (XRD) data. The energy-dispersive X-ray spectroscopy (EDX) technique was used to verify the chemical compositions. The isothermal and isofield magnetic measurements were carried out by using the Quantum Design Physical Property Measurement System (PPMS).

2. Experimental details

The polycrystalline PSMO samples were prepared by using the solid-state reaction method. The use of the latter for synthesizing manganites and composite materials seems to be the most convenient since it has good grain growth distribution, excellent process control, and appropriate process time. Stoichiometric proportions of Pr_6Sr_{11}, SrO, and MnO_2 powders with high purity were mixed and grounded in an agate mortar for 1 hour. The mixture was annealed at 1000 °C for 12h and at 1200 °C for 24h in air, with intermediate grinding. Then, the calcined powder was divided into four equal quantities. PSMO (2h HT) and PSMO (24h HT) samples were heat-treated for two hours and 24 hours, respectively, at 1200 °C. The two remaining quantities were used to prepare the PSMO-CuO composites,

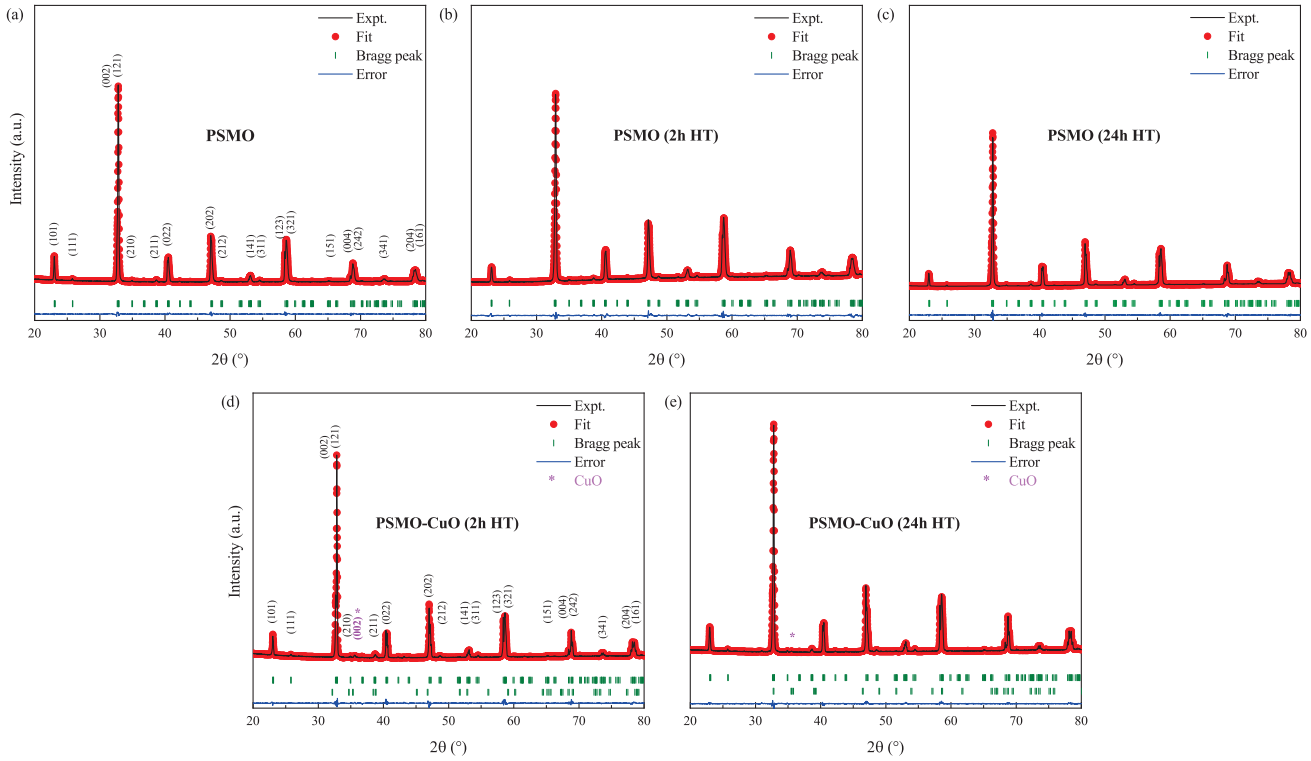

Fig. 1: XRD patterns for (a) PSMO, (b) PSMO (2h HT), (c) PSMO (24h HT), (d) PSMO-CuO (2h HT), and (e) PSMO-CuO (24h HT) polycrystalline.

Table 1: Rietveld refined lattice constants, unit cell volume, bond angles, bond lengths and MnO_6 octahedron structural characteristics of both pristine and composite samples in case of presence and absence of additional heat treatment. XRD data were obtained at room temperature.

Compound	a (Å)	b (Å)	c (Å)	$c/\sqrt{2}$ (Å)	V (Å^3)	Mn-O_I-Mn (°)	Mn-O_{II}-Mn (Å)	Mn-O_I (Å)	<Mn-O_{II}>	<ω>	$W_{Mn-O_{II}-Mn}$
PSMO	5.480	5.449	7.701	5.445	229.956	157.964	163.239	1.961	1.953	19.399	0.0950
PSMO (2h HT)	5.490	5.458	7.714	5.455	231.146	157.440	162.611	1.966	1.958	19.975	0.0941
PSMO (24h HT)	5.486	5.452	7.704	5.448	230.424	158.930	162.018	1.959	1.958	19.526	0.0940
PSMO-CuO (2h HT)	5.482	5.449	7.698	5.443	229.950	158.988	156.121	1.957	1.975	22.446	0.0904
PSMO-CuO (24h HT)	5.486	5.452	7.701	5.445	230.334	160.029	157.838	1.955	1.970	21.067	0.0915

where a small quantity of copper oxide (5% weight ratio) was added and well mixed with PSMO to have a homogenous powder. The resulting mixtures denoted as PSMO-CuO (2h HT) and PSMO-CuO (24h HT) were calcined at 1200 °C for 2h and 24h, respectively. To check the crystalline quality of prepared samples, XRD measurements were performed at room temperature using a Bruker D8 ADVANCE diffractometer with Cu-Kα radiation over the 2θ-angular range of $10° < 2\theta < 80°$ with a step size of 0.01°. The particle sizes and the surface morphology were analyzed by employing an Analytical Scanning Electron Microscope (ASEM) model X. Magnetization data were collected over the temperature range of 10–350 K under magnetic fields going from 0 to 7 T by using a superconducting quantum interference device magnetometer from Quantum Design, model MPMS XL.

3. Results and discussion

3.1. Structural characterization

The X-ray diffraction patterns of PSMO (2h HT - 24h HT) and PSMO-CuO (2h HT - 24h HT) samples at room temperature are shown in Fig. 1. HighScore Plus software was used to analyze the existing phases, and the Rietveld method was adopted to refine the XRD data using the FullProf refinement software [86, 87]. The observed and calculated patterns are successfully superposed with a reliability factor (R_{WP}) less than 7%, unveiling the excellent quality of refinement [88]. The analysis of XRD data as reported in Fig. 1 shows that the compounds are single phased without any impurities. This means that no additional phases (e.g., Mn_3O_4, Mn_5O_8, Pr_6O_{11}) and/or no additional impurities at the Mn sites (e.g., Cr, Co, Fe, Ni) can be found other than PSMO in the pristine samples and PSMO-CuO in the composite samples. At room temperature, PSMO samples are well crystallized in the orthorhombic structure with the Pbnm (n° 62) space group. For the PSMO-CuO samples, the coexistence of copper oxide and PSMO can be clearly observed with a strong orientation along the (200) direction. The refinement results for the studied samples are summarized in Table 1.

The XRD data examination revealed that adding a small amount of CuO to the pristine PSMO led to a minor modification in the lattice constants and the cell volume. Moreover, it is worthy to mention that for all studied samples, $c/\sqrt{2} < b < a$. However, the addition of CuO resulted in a significant change in the Mn-O_{II}-Mn bond angle that decreases from about 162° for PSMO to about 156° for PSMO in the composite samples. The average Mn–O–Mn bond angle distortion of MnO_6

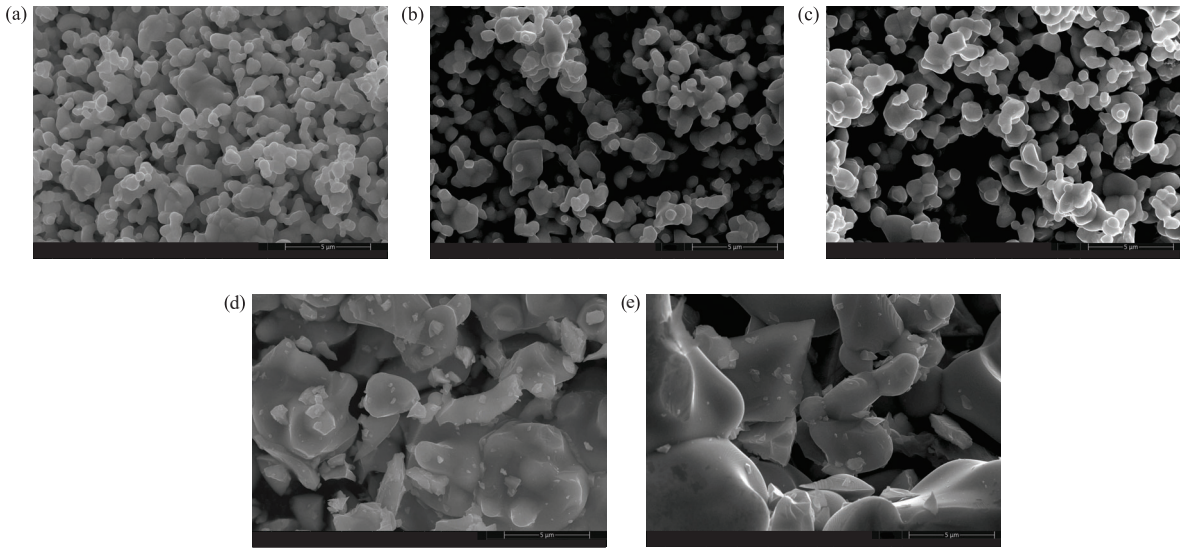

Fig. 2: Scanning electron micrograph (SEM) of (a) PSMO, (b) PSMO (2h HT), (c) PSMO (24h HT), (d) PSMO-CuO (2h HT), and (e) PSMO-CuO (24h HT) samples.

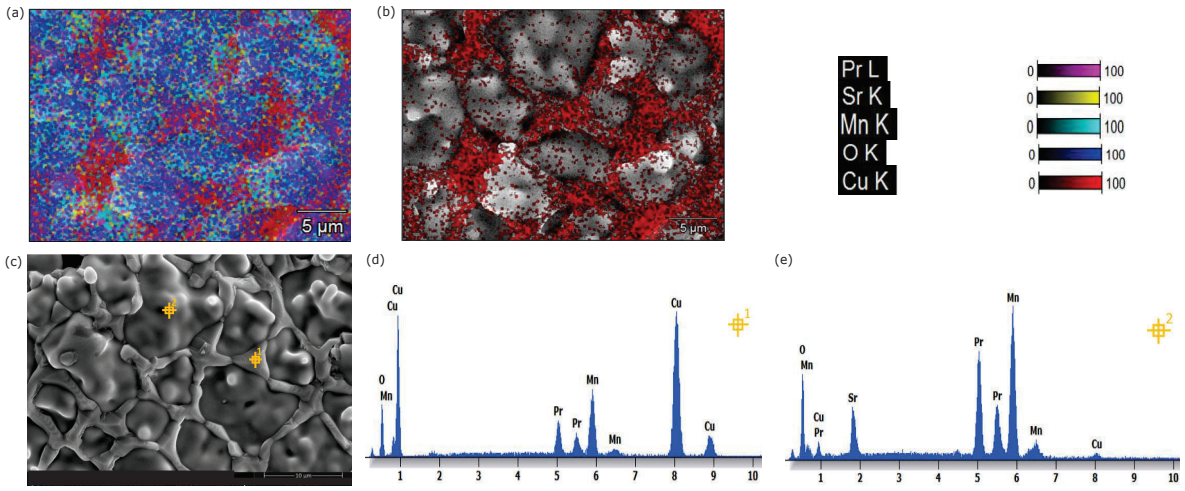

Fig. 3: Elemental mapping for PSMO-CuO (24h HT) with (a) all present elements and (b) only copper element. (c) SEM micrographs of PSMO-CuO (24h HT) and their associated EDX spectrum at: (d) the grains boundaries and (e) the grains surface.

octahedra in the studied samples is defined as $<\omega> = 180° - <\text{Mn-O-Mn}>$ [78, 89]. From Table 1, it is noticed that the value of $< \omega >$ increases when adding the CuO secondary phase, indicating that the latter enhances the octahedral MnO_6 distortion. Moreover, the variation in bond angles and lengths leads to a change in the effective one-electron bandwidth $W_{Mn-O-Mn}$ (electron hopping interaction for Mn^{3+} and Mn^{4+} ions), described as [90],

$$W_{\text{Mn-O-Mn}} \propto \frac{\cos\left(\frac{\pi - \theta_{\text{Mn-O-Mn}}}{2}\right)}{d^{3.5}_{\text{Mn-O}}}, \quad (1)$$

where $\theta_{\text{Mn-O-Mn}}$ is the Mn-O-Mn bond angle, whereas $d_{\text{Mn-O}}$ represents the Mn-O bond length. Table 1 includes the estimated values of W, which decreases for the composite samples as compared to pristine ones. The narrowing of the one-electron bandwidth indicates that the double exchange (Mn^{3+}-O^{2-}-Mn^{4+}) interaction is less dominant than the superexchange (Mn^{3+}-O^{2-}-Mn^{3+}) coupling or other electronic instabilities [91]. Additionally, the lower $W_{Mn-O-Mn}$ implies a possible weakening of the octahedron electron transition probability.

On the other hand, scanning electron micrographs of the studied samples are reported in Fig. 2. The surface of obtained pure PSMO perovskite powders after the three heat treatment modes, shown in Fig. 2(a, b, and c), is composed of almost accumulated spherical grains with an average grain size of 0.6 μm and a homogeneous microstructure. It is worth mentioning that the addition of two or twenty-four hours of heat treatment has no effect on the grain size. However when the CuO phase is mixed with the pristine compound under the same heat treatment conditions, the PSMO grains began to merge together, while their boundaries became challenging to detect due to their large size as can be seen in Fig. 2(d and e). The CuO effect is readily apparent in the PSMO mean grain size that markedly increases from 0.6 μm to 5 μm. More results concerning the scanning electron micrograph and elemental mapping of here investigated samples, as well as their associated EDX spectrum, are provided in the supplementary information (see Figure S1).

To get insight on the location of CuO, a plate form is made for the composite powder. The elemental analyses of the PSMO-CuO pellet were carried out by EDX micro-analysis and reported in Fig. 3. The latter shows the presence of a large quantity of Cu metal at the grain boundaries, corresponding to about 45% of the atomic ratio. However, the Cu concentration is only about 1% at the grains surface, which is mainly composed of Pr, Sr, Mn, and O chemical elements. These findings reveal that the copper oxide which covers the pure material grains markedly promoted grain growth because of the liquid sintering [75, 83, 92], since the melting point of CuO (1325 °C) is close to the sintering temperature (1200 °C).

3.2. Magnetic properties

To better understand the effect of secondary phase and additional heat treatments on the magnetic properties of studied samples, it is necessary to investigate their temperature dependence of magnetization. Thus, in Fig. 4(a), the latter is shown for both pristine and composite samples. The measurements reveal that the magnetization of investigated materials under a magnetic field of 0.1 T rapidly changes near their Curie temperature. The magnetic phase transition from the ordered (ferromagnet) to the disordered (paramagnet) state takes place at high temperatures, which is mainly due to the strong double exchange $Mn^{3+}(t^3_{2g}\ e^1_g)$-O^{2-}(2p)-$Mn^{4+}(t^3_{2g}\ e^0_g)$ interaction [32].

Furthermore, the Curie temperature can be determined from the lowest value of the dM/dT versus T curves. As shown in Fig. 4(b), the T_c of composite materials is around 273 K, which is significantly lower than that of the PSMO sample T_c = 293 K. Based on the double exchange model, a lower T_c indicates a loss of overlap between the Mn(3d) and O(2p) orbitals [57], which can be confirmed by the decreased effective one electron bandwidth $W_{Mn-O-Mn}$ for composite samples as reported in Table 1.

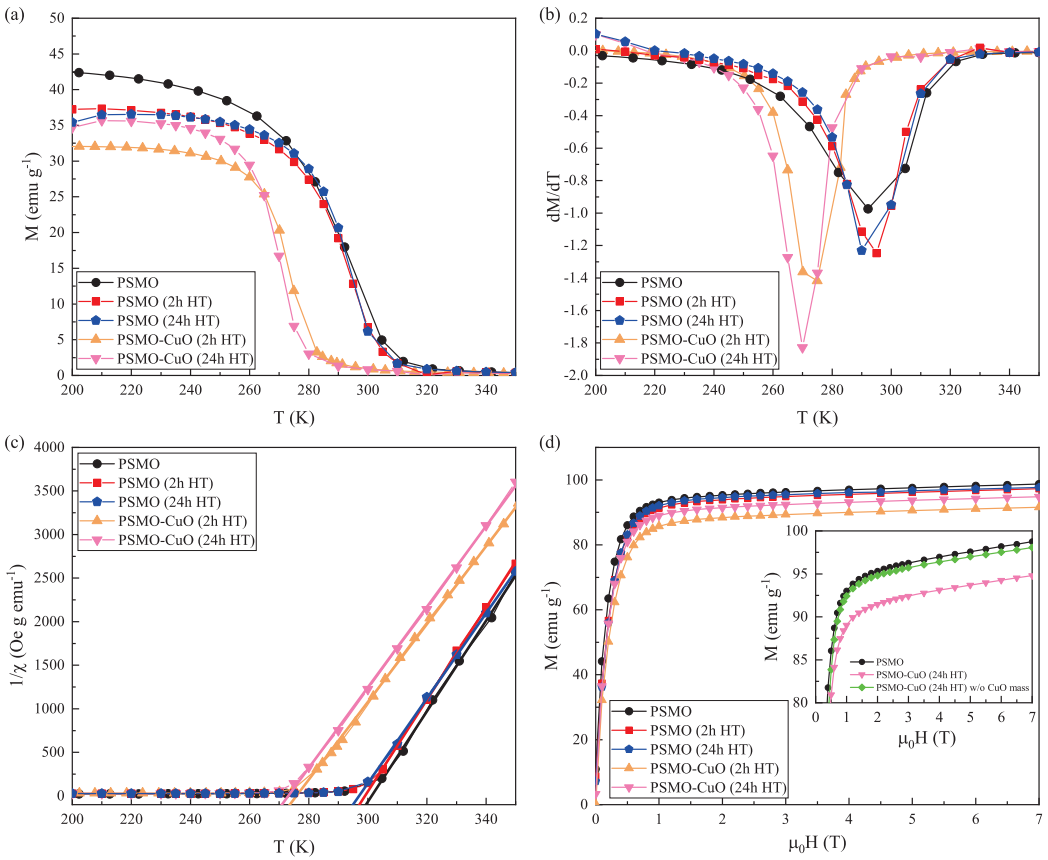

Fig. 4: (a) Temperature-dependent magnetization under a magnetic field of 0.1 T. (b) Plots of dM/dT versus temperature for 0.1 T. (c) The temperature-dependent inverse susceptibility for 0.1 T of both pristine and composite samples. (d) Isothermal magnetization curve at 10 K. The inset figure represents the magnetization at 10 K for the PSMO, PSMO-CuO (24h HT) and PSMO-CuO (24h HT) without accounting the CuO mass in the calculation.

The inverse susceptibility (χ^{-1}) as function of temperature is represented in Fig. 4(c). From the Curie-Weiss fitted plots, we can see that above the Curie temperature, the susceptibility obeys the Curie-Weiss law, defined as,

$$\chi = \frac{C}{\mathrm{T} - \mathrm{T}_\theta}, \tag{2}$$

where T_θ is the Curie-Weiss temperature, and C is the Curie constant that can be determined by the linear fit of χ^{-1}. The obtained Curie constants can be further used to deduce the experimental effective magnetic moment, using the following equation [93],

$$\mu_{eff}^{exp} = \sqrt{\frac{3 \cdot C \cdot k_B \cdot M_m}{N_a}}\,\mu_B, \tag{3}$$

where μ_B is the Bohr magneton, k_B is the Boltzmann constant, N_a is the Avogadro number, and M_m is the molecular formula weight. The obtained experimental values are summarized in Table 2. Moreover, the theoretical effective magnetic moment of $Pr_{1-x}Sr_xMnO_3$ can be obtained using the following relation [79],

$$\mu_{eff}^{theo} = \sqrt{(1-x)\cdot\mu_{eff}^2(\mathrm{Pr}^{3+}) + (1-x)\cdot\mu_{eff}^2(\mathrm{Mn}^{3+}) + x\cdot\mu_{eff}^2(\mathrm{Mn}^{4+})}, \tag{4}$$

where $\mu_{eff}(Pr^{3+})$, $\mu_{eff}(Mn^{3+})$, and $\mu_{eff}(Mn^{4+})$ represents the effective magnetic moment of Pr^{3+}, Mn^{3+}, and Mn^{4+} ions, respectively. $Pr_{2/3}Sr_{1/3}MnO_3$ has a theoretical effective magnetic moment of 5.44 μ_B. The higher experimental value of μ_{eff} compared with the theoretical value can be related to the presence of the FM state above T_c [94, 95]. Furthermore, at 10 K, Fig. 4(d) depicts the magnetization variation as a function of magnetic field. PSMO has a greater magnetization value than the other composite samples, which is primarily due to the decreased FM volume caused by the introduction of CuO. This is confirmed by the magnetization of the composite that is approximately equal to that of the pure sample when removing the contribution of secondary phase, as can be seen in the inset of Fig. 4(d).

The isothermal magnetization M(H) curves recorded in the temperature range going from 250 K to 310 K and under changing magnetic fields up to 7 T for both pristine and composite samples are reported in Fig. 5. At low temperatures, the magnetization curves exhibit a nonlinear pattern with a tendency to saturate in the presence of magnetic fields, indicating a ferromagnetic behavior. However, above T_c, the magnetization evolves almost linearly, indicating a paramagnetic state caused by the thermal agitation disrupting the arrangement of magnetic moments.

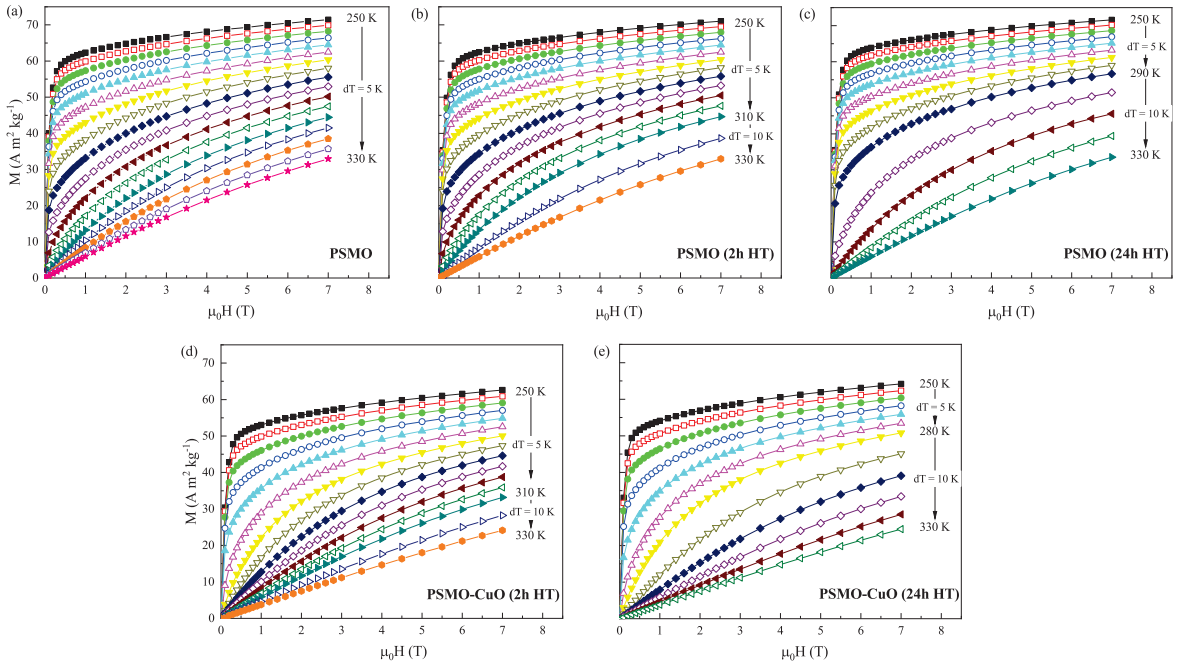

Fig. 5: Isothermal magnetization curves for the investigated samples at different temperatures close to the magnetic phase transition and up to 7 T.

3.3. Magnetocaloric properties

This work also aims to determine the magnetocaloric properties of studied samples. In this way and according to the Arrott plots (M^2 versus H/M) presented in Figure S2, the positive slope of the curves indicates on the occurrence of a second-order magnetic transition in all studied materials [96]. Therefore, for materials that show a second-order transition and very low field hysteresis, which is the case of the here investigated $Pr_{2/3}Sr_{1/3}MnO_3$ oxide and its composite, the isothermal entropy change resulting from the variation of external magnetic fields from 0 to H can be obtained by using the following Maxwell relation [8, 97, 98],

$$\Delta S\,(T, 0 \rightarrow H) = \int_0^H \left(\frac{\partial M}{\partial T}\right)_{H'} dH', \tag{5}$$

where ΔS is determined numerically by using the numerical form of above equation and reported magnetic isotherms in Fig. 5. In this case, ΔS is given by,

$$\Delta S = \sum_i \frac{M_{i+1} - M_i}{T_{i+1} - T_i} \Delta H_i, \tag{6}$$

where M_{i+1} and M_i are the measured magnetization under an external magnetic field at T_{i+1} and T_i, respectively. In Fig. 6(c), the change in magnetic entropy as a function of temperature for all studied samples under some representative magnetic fields is reported. Their entropy change exhibits a maximum close to Curie temperatures and then drops almost symmetrically beyond the phase transition region. The ΔS maximum values increases from 1.32 to 5.77 J kg^{-1} K^{-1} and from 1.88 to 6.23 J kg^{-1} K^{-1} when increasing the applied magnetic field from 1 T to 7 T for PSMO and PSMO-CuO, respectively, while keeping their location at T_c as shown in Fig. 6(a-b). On the other hand, when the magnetic field is varied by 4 T, the highest magnetic entropy change for PSMO-CuO approaches 4.66 J kg^{-1} K^{-1} (at 273 K), whereas for PSMO it is roughly equal to 3.7 J kg^{-1} K^{-1} (at 293 K). This difference is due mainly to the fact that the magnetic phase transition of the PSMO-CuO compound is broader than that of the pure compound. As mentioned above, the here investigated manganite shows relatively lower ΔS value when compared with gadolinium (Gd), which exhibits a large entropy change value of 2.8 J kg^{-1} K^{-1} (at 292 K) under a magnetic field of 1 T [13]. However, when compared with similar oxides such as $La_{2/3}(Ca_{0.75}Sr_{0.25})_{1/3}MnO_3$, which is considered as the best candidate among manganites for near-room temperature magnetic refrigeration, the PSMO-CuO sample exhibits a similar magnetic entropy change [99]. Nevertheless, ΔS can be remarkably enhanced for here investigated manganite oxides when an appropriate method of preparation

Table 2: Curie temperature (T_c), Curie-Weiss temperature (T_θ), Curie constant (C), and experimental magnetic moment $\left(\mu_{eff}^{exp}\right)$ obtained from magnetization data for all studied samples.

Sample	T_c (K)	T_θ (K)	C	μ_{eff}^{exp} (μ_B)
PSMO	293	300	0.0192	5.89
PSMO (2h HT)	295	299	0.0189	5.84
PSMO (24h HT)	291	297	0.0205	6.08
PSMO-CuO (2h HT)	274	276	0.0223	6.35
PSMO-CuO (24h HT)	270	273	0.0216	6.24

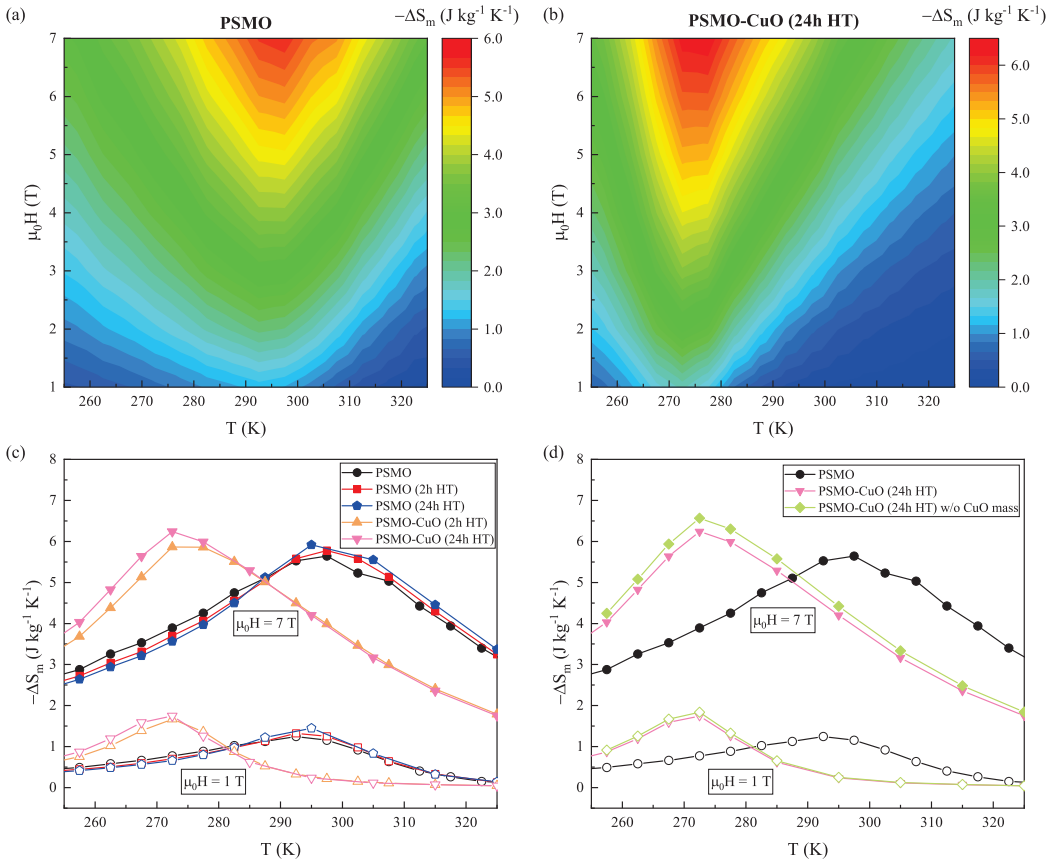

Fig. 6: 2D contour plots of the magnetic entropy changes as function of temperature and magnetic field for (a) PSMO and (b) PSMO-CuO (24h HT). (c) Magnetic entropy changes as function of temperature for the investigated samples under a magnetic field of 1 T (open symbols) and 7 T (solid symbols). (d) Magnetic entropy changes as function of temperature for PSMO, PSMO-CuO (24h HT) and PSMO-CuO (24h HT) without accounting the CuO mass in the calculation.

is used. In fact, Phan et al. [76] have prepared a single crystal $Pr_{0.63}Sr_{0.37}MnO_3$ which exhibits a high magnetic entropy change of 2.57 J kg^{-1} K^{-1} (at 305 K) under a magnetic field of 1 T. Furthermore, when the $Pr_{0.63}Sr_{0.37}MnO_3$ is shaped into a pellet form with a higher calcination temperature and duration, the magnetic entropy change could also be enhanced according to Ref. [33]. Fig. 6(d) represent the magnetic entropy changes of PSMO, PSMO-CuO (24h HT) and PSMO-CuO (24h HT), without considering the mass contribution of CuO as a function of temperature under some representative magnetic fields. As can be seen, a slight increase in the entropy change that attains 1.9 J kg^{-1} K^{-1} (1 T) is observed. The latter is considered as the real ΔS_{m} value of PSMO magnetic entropy change in the PSMO-CuO composite material, as the CuO secondary phase has no contribution to the total magnetization and accordingly the MCE. In addition to the entropy change, the refrigerant capacity (RC) is an important parameter that describes the efficiency of a magnetocaloric material. In fact, materials with a higher RC are more suitable for practical applications. RC is given by [100],

$$\mathrm{RC} = -\int_{T_{cold}}^{T_{hot}} \Delta S_m(T)\, dT, \tag{7}$$

where T_{cold} and T_{hot} are the respective temperatures at the ΔS_m peak's full width half maximum, which can be calculated numerically by integrating the area under the ΔS_m versus T curve between T_{cold} and T_{hot}. In Fig. 7, the RC values are plotted versus the applied magnetic field. As can be seen, the RC linearly increases with magnetic field reaching 40 J kg^{-1} and 308 J kg^{-1} for PSMO, and 32 J kg^{-1} and 271 J kg^{-1} for PSMO-CuO under 1 T and 7 T, respectively. The observed decrease in RC regarding the PSMO-CuO is particularly due to the reduction of its working temperature range as the magnetic phase transition is closer to the first order transition character. On the other hand, the resulting RC is nearly similar to that of the near-room temperature refrigerant $La_{2/3}(Ca_{0.75}Sr_{0.25})_{1/3}MnO_3$ (RC = 37 J kg^{-1}) [99]. However, when compared to other high-performance magnetic refrigerants such as Gd (RC = 170.17 J kg^{-1} for 2 T) and $LaFe_{13-x}Si_x$ (RC = 97.05 J kg^{-1} for 2 T) based compounds, the studied materials exhibit relatively lower values.

Various studies have demonstrated the strong interplay between lattice and spin degrees of freedom in perovskite-type manganese oxides [101]. Therefore, a variety of mechanisms may explain the reduction in transition temperature and the variation

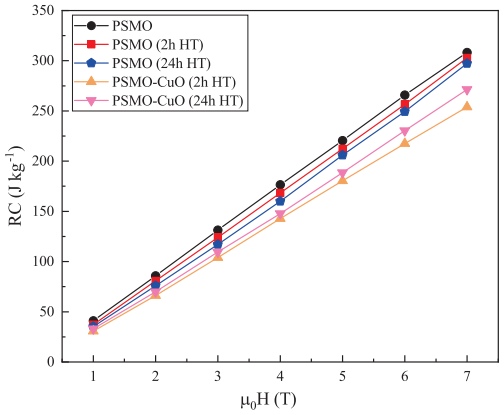

Fig. 7: Refrigerant capacity versus applied magnetic field for PSMO and PSMO-CuO samples.

of PSMO-CuO magnetic entropy. First, the insertion of CuO phase in the PSMO matrix weakens the FM interaction through structural modifications. In fact, the presence of this secondary phase in the grain boundaries leads to an apparent structural deformation in the primary phase where the Mn-O bond distances and Mn-O-Mn bond angles are significantly affected as reported in Table 1. In fact, the loss in FM interactions can be explained by the weaker double exchange mechanism caused by the reduction in the Mn-O-Mn bond angle since the amplitude of charge carriers hopping from one Mn ion to another is reduced when this angle deviates from 180° [36, 102–104]. Accordingly, the remarkable decrease in the Curie temperature is expected based on the following relation [105],

$$T_c \simeq \frac{\cos(\varphi)}{d_{Mn-O}}, \tag{8}$$

where d_{Mn-O} is the length of the Mn-O bond and φ is the Mn-O-Mn bond angle. The observed modification in φ can be explained by a tensile force exerted by the CuO secondary phase, particularly near grain boundaries. Furthermore, the loss in ferromagnetic interactions can be also reinforced by the low magnetic coupling between the grains due to the inter-grain constructed layer (CuO phase), which is magnetically different from the magnetic state of the grains [106].

On the other hand, even though there is only an additional 2 hours of heat treatment at 1200 °C to PSMO-CuO, this brief period was good enough to markedly increase the grain size as shown in Fig. 2. This is because of the presence of CuO, which acts as a sintering aid. In Park et al. [107] study, it was demonstrated that the magnetization at the surface boundary of the manganese oxide $La_{0.7}Sr_{0.3}MnO_3$ decays much slower than the bulk magnetization. Therefore, the high grain size of the composite samples may promote a more ordered FM phase and, consequently, reduce the magnetic transition width (i.e. more pronounced magnetic phase transition) since the impact from the magnetically disordered surface boundary is reduced, which can explain the slight increase of the magnetic entropy. On the other hand, the near first-order magnetic transition may also be related to the significant decrease in the Curie temperature. With regards to the effect of additional heat treatments on magnetic and magnetocaloric properties, the obtained results indicate that, in the absence or the presence of secondary phase, the Curie temperature and the magnetic entropy change are almost constant. Therefore, the additional heat treatment has no effect on the magnetic and magnetocaloric properties since the observed modifications in the composite samples are in fact directly arises from the added secondary phase.

4. Multilayered magnetocaloric refrigerants based on PSMO and PSMO-CuO

As already reported in this study, the investigated manganite oxides show a significant magnetocaloric effect that remains peaked on a relatively narrow temperature range, which is not appreciated from a practical point of view. However, as demonstrated above, the addition of CuO as secondary phase to the pristine PSMO enables us to reduce its Curie temperature to

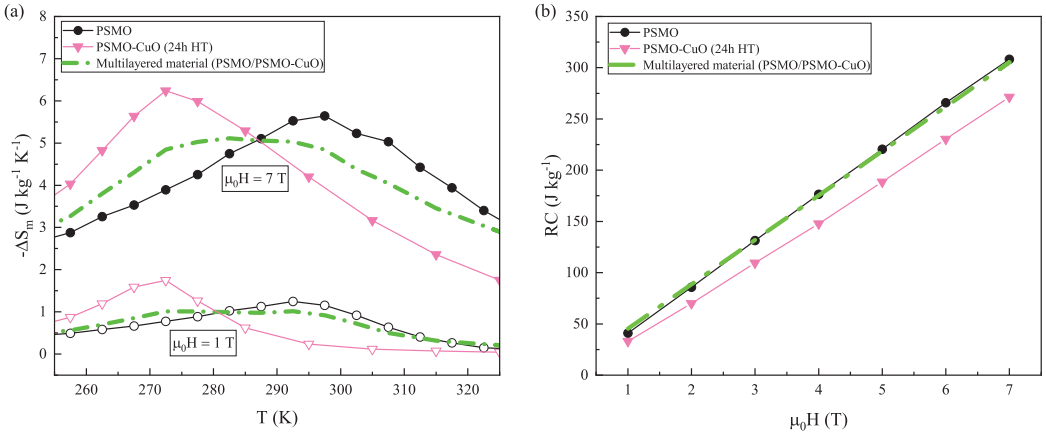

Fig. 8: (a) Magnetic entropy changes of PSMO, PSMO-CuO (24h HT), and the multilayered material composed of both PSMO and PSMO-CuO (24h HT) samples as function of temperature under magnetic fields of 1 T and 7 T. (b) Magnetic refrigeration capacity (RC) versus applied magnetic field for PSMO, PSMO-CuO (24h HT) and the multilayered material.

about 273 K without proceeding to doping effects. Taking advantage of such a result, a multilayered refrigerant based on both PSMO and PSMO-CuO is proposed aiming to cover a wide temperature range close to ambient temperature. The proposed multilayered material can be employed as a refrigerant in cooling devices that use AMR and Ericsson cycles to achieve the refrigeration process. The latter cycle particularly requires a constant entropy change over the considered temperature range [8, 108–114]. For this purpose, the numerical method proposed in Refs. [109, 115] was used to identify the optimum mass ratio, y_i, for each material based on the isothermal entropy change represented in Fig. 6. In general, for a refrigerant constituted of n magnetic compounds, the resulting isothermal entropy change can be given by the following relation,

$$\Delta S_{com} = \sum_{i=1}^{n} y_i \Delta S_i, \tag{9}$$

where y_i is the mass proportion of one of the constituent compounds. If ΔS_{com} of the composite material utilized as the working substance in the Ericsson refrigeration cycle is maintained constant across a specified temperature range, the refrigeration cycle may achieve a complete regeneration [114]. In this case, Eq. (9) can be expressed as follows,

$$\Delta S_{Com} = \sum_{i=1}^{n} y_i \left[\Delta S_i\left(T_c^{j+1}\right) - \Delta S_i\left(T_c^{j}\right)\right] = 0, \tag{10}$$

where j = 1,2,..., n-1 and T_c is the Curie temperature of ith constituent material. Under a magnetic fields of 1 T and 7 T, the optimum mass ratio of the considered materials is determined using the combination of Eq. (10) and the fact that $\sum_{i=1}^{n} y_i = 1$. The calculated ΔS_{com} versus temperature and magnetic field is shown in Fig. 8(a). As can be observed, ΔS_{com} remains almost constant within the temperature range 273–293 K. Indeed, a nearly perfect plateau is observed in the multilayered isothermal entropy change curve with an average value of 1 J kg^{-1} K^{-1} (1 T) and 5.11 J kg^{-1} K^{-1} (7 T). Even though the achieved ΔS_{com} is lower than the one of the constituent samples, the broadening of the working temperature makes the proposed composite material a potential working substance in magnetic refrigeration cycles. Similar features were reported by Balli et al. [112] and Smaili et al. [111] for a composite refrigerant based on $Gd_{1-x}Tb_x$ and $Gd_{1-x}Dy_x$ alloys, where it is observed that ΔS_{com} remains practically constant for near-room temperatures range of (260–300 K) and (210-290 K), respectively, with higher magnetic entropy change when compared to the here investigated materials. Furthermore, as shown in Fig. 8(b), the magnetic refrigeration capacity of the multilayered system is greater than that of the composite material, and approximately equivalent to that of pure PSMO.

5. Conclusions

To sum up, the structural, magnetic, and magnetocaloric properties of $Pr_{2/3}Sr_{1/3}MnO_3$ (PSMO) and $Pr_{2/3}Sr_{1/3}MnO_3$(95%)-CuO(5%) (PSMO-CuO) samples have been studied to particularly assess the real impact of the added CuO secondary phase on the magnetic and magnetocaloric features of PSMO. Therefore, the bond lengths and angles of prepared samples were determined by the Rietveld refinement method of the X-ray data. The latter unveil a significant variation in the Mn-O-Mn bond angles caused by the tensile strain resulting from the secondary phase located at the grain boundaries. This was confirmed by using SEM micrographs. Moreover, such structural deformations weaken the ferromagnetic interactions controlled by double-exchange couplings, which markedly decrease the Curie temperature from 293 K for the pristine PSMO to about 273 K for the PSMO-CuO composite. This is associated with the enhancement of the magnetocaloric effect in the PSMO-CuO. Based on the obtained results, a multilayered refrigerant based on PSMO and PSMO-CuO materials is proposed for room temperature magnetic cooling applications. The resulting entropy change remains nearly constant over the temperature range going from 273 K to 293 K, being a favorable situation for the efficient AMR and Ericsson thermodynamic cycles.

Acknowledgments

O. Chdil and M. Balli acknowledge funding by the International University of Rabat. The authors would like to thank S. Pelletier and B. Rivard for the technical support. We acknowledge the financial support from NSERC (Canada), FQRNT (Québec), CFI, Canada First Research Excellence Fund (Apogée Canada), and Université de Sherbrooke. The authors gratefully acknowledge MAScIR foundation for providing the experimental facilities.

References

[1] K. Gschneidner Jr, V. Pecharsky, Thirty years of near room temperature magnetic cooling: Where we are today and future prospects, International journal of refrigeration 31 (6) (2008) 945–961.

[2] O. Gutfleisch, M. A. Willard, E. Brück, C. H. Chen, S. Sankar, J. P. Liu, Magnetic materials and devices for the 21st century: stronger, lighter, and more energy efficient, Advanced materials 23 (7) (2011) 821–842.

[3] J. Liu, T. Gottschall, K. P. Skokov, J. D. Moore, O. Gutfleisch, Giant magnetocaloric effect driven by structural transitions, Nature materials 11 (7) (2012) 620–626.

[4] M. Balli, O. Sari, C. Mahmed, C. Besson, P. Bonhote, D. Duc, J. Forchelet, A pre-industrial magnetic cooling system for room temperature application, Applied Energy 98 (2012) 556–561.

[5] K. Engelbrecht, D. Eriksen, C. Bahl, R. Bjørk, J. Geyti, J. Lozano, K. K. Nielsen, F. Saxild, A. Smith, N. Pryds, Experimental results for a novel rotary active magnetic regenerator, International Journal of Refrigeration 35 (6) (2012) 1498–1505.

[6] X. Moya, L. Hueso, F. Maccherozzi, A. Tovstolytkin, D. Podyalovskii, C. Ducati, L. Phillips, M. Ghidini, O. Hovorka, A. Berger, et al., Giant and reversible extrinsic magnetocaloric effects in $La_{0.7}Ca_{0.3}MnO_3$ films due to strain, Nature materials 12 (1) (2013) 52–58.

[7] A. M. Tishin, Y. I. Spichkin, The magnetocaloric effect and its applications, CRC Press, 2016.

[8] M. Balli, S. Jandl, P. Fournier, A. Kedous-Lebouc, Advanced materials for magnetic cooling: Fundamentals and practical aspects, Applied Physics Reviews 4 (2) (2017) 021305.

[9] B. Yu, M. Liu, P. W. Egolf, A. Kitanovski, A review of magnetic refrigerator and heat pump prototypes built before the year 2010, International Journal of refrigeration 33 (6) (2010) 1029–1060.

[10] F. Scarpa, G. Tagliafico, L. A. Tagliafico, A classification methodology applied to existing room temperature magnetic refrigerators up to the year 2014, Renewable and Sustainable Energy Reviews 50 (2015) 497–503.

[11] A. Kitanovski, U. Plaznik, U. Tomc, A. Poredoš, Present and future caloric refrigeration and heat-pump technologies, International Journal of Refrigeration 57 (2015) 288–298.

[12] A. Smith, C. R. Bahl, R. Bjørk, K. Engelbrecht, K. K. Nielsen, N. Pryds, Materials challenges for high performance magnetocaloric refrigeration devices, Advanced Energy Materials 2 (11) (2012) 1288–1318.

[13] T. Gottschall, K. P. Skokov, M. Fries, A. Taubel, I. Radulov, F. Scheibel, D. Benke, S. Riegg, O. Gutfleisch, Making a cool choice: the materials library of magnetic refrigeration, Advanced Energy Materials 9 (34) (2019) 1901322.

[14] A. Kitanovski, Energy applications of magnetocaloric materials, Advanced Energy Materials 10 (10) (2020) 1903741.

[15] V. Franco, J. Blázquez, B. Ingale, A. Conde, The magnetocaloric effect and magnetic refrigeration near room temperature: materials and models, Annual Review of Materials Research 42 (2012) 305–342.

[16] N. De Oliveira, P. J. von RANKE, Theoretical aspects of the magnetocaloric effect, Physics Reports 489 (4-5) (2010) 89–159.

[17] O. Tegus, E. Brück, K. Buschow, F. De Boer, Transition-metal-based magnetic refrigerants for room-temperature applications, Nature 415 (6868) (2002) 150–152.

[18] N. Terada, H. Mamiya, High-efficiency magnetic refrigeration using holmium, Nature communications 12 (1) (2021) 1–6.

[19] V. Franco, J. Blázquez, J. Ipus, J. Law, L. Moreno-Ramírez, A. Conde, Magnetocaloric effect: From materials research to refrigeration devices, Progress in Materials Science 93 (2018) 112–232.

[20] R. Gimaev, Y. Spichkin, B. Kovalev, K. Kamilov, V. Zverev, A. Tishin, Review on magnetic refrigeration devices based on htsc materials, International Journal of Refrigeration 100 (2019) 1–12.

[21] M. S. Kamran, H. O. Ahmad, H. S. Wang, Review on the developments of active magnetic regenerator refrigerators–evaluated by performance, Renewable and Sustainable Energy Reviews 133 (2020) 110247.

[22] T. Krenke, E. Duman, M. Acet, E. F. Wassermann, X. Moya, L. Mañosa, A. Planes, Inverse magnetocaloric effect in ferromagnetic Ni-Mn-Sn alloys, Nature materials 4 (6) (2005) 450–454.

[23] A. Barman, S. Kar-Narayan, D. Mukherjee, Caloric effects in perovskite oxides, Advanced Materials Interfaces 6 (15) (2019) 1900291.

[24] N. A. Zarkevich, V. I. Zverev, Viable materials with a giant magnetocaloric effect, Crystals 10 (9) (2020) 815.

[25] Y. Zhang, J. Wu, J. He, K. Wang, G. Yu, Solutions to obstacles in the commercialization of room-temperature magnetic refrigeration, Renewable and Sustainable Energy Reviews 143 (2021) 110933.

[26] C. R. Bahl, D. Velázquez, K. K. Nielsen, K. Engelbrecht, K. B. Andersen, R. Bulatova, N. Pryds, High performance magnetocaloric perovskites for magnetic refrigeration, Applied Physics Letters 100 (12) (2012) 121905.

[27] M. Balli, B. Roberge, P. Fournier, S. Jandl, Review of the magnetocaloric effect in $RMnO_3$ and RMn_2O_5 multiferroic crystals, Crystals 7 (2) (2017) 44.

[28] V. Chaudhary, X. Chen, R. V. Ramanujan, Iron and manganese based magnetocaloric materials for near room temperature thermal management, Progress in Materials Science 100 (2019) 64–98.

[29] M.-H. Phan, S.-C. Yu, Review of the magnetocaloric effect in manganite materials, Journal of Magnetism and Magnetic Materials 308 (2) (2007) 325–340.

[30] D. T. Morelli, A. M. Mance, J. V. Mantese, A. L. Micheli, Magnetocaloric properties of doped lanthanum manganite films, Journal of applied physics 79 (1) (1996) 373–375.

[31] Z. Guo, Y. Du, J. Zhu, H. Huang, W. Ding, D. Feng, Large magnetic entropy change in perovskite-type manganese oxides, Physical review letters 78 (6) (1997) 1142.

[32] J. Coey, M. Viret, S. Von Molnar, Mixed-valence manganites, Advances in physics 48 (2) (1999) 167–293.

[33] F. Guillou, U. Legait, A. Kedous-Lebouc, V. Hardy, Development of a new magnetocaloric material used in a magnetic refrigeration device, in: EPJ Web of Conferences, Vol. 29, EDP Sciences, 2012, p. 00021.

[34] C. Zener, Interaction between the d-shells in the transition metals. ii. ferromagnetic compounds of manganese with perovskite structure, Physical Review 82 (3) (1951) 403.

[35] P. W. Anderson, H. Hasegawa, Considerations on double exchange, Physical Review 100 (2) (1955) 675.

[36] T. Kaplan, S. Mahanti, Physics of manganites, Springer Science & Business Media, 2006.

[37] D. Rocco, A. Coelho, S. Gama, M. d. C. Santos, Dependence of the magnetocaloric effect on the A-site ionic radius in isoelectronic manganites, Journal of Applied Physics 113 (11) (2013) 113907.

[38] K. Ahn, X. Wu, K. Liu, C. Chien, Magnetic properties and colossal magnetoresistance of La(Ca)MnO_3 materials doped with Fe, Physical Review B 54 (21) (1996) 15299.

[39] R. Thaljaoui, W. Boujelben, M. Pękała, K. Pękała, J.-F. Fagnard, P. Vanderbemden, M. Donten, A. Cheikhrouhou, Magnetocaloric effect of monovalent K doped manganites $Pr_{0.6}Sr_{0.4-x}K_xMnO_3$ (x= 0 to 0.2), Journal of magnetism and magnetic materials 352 (2014) 6–12.

[40] R. M'nassri, N. C. Boudjada, A. Cheikhrouhou, Impact of sintering temperature on the magnetic and magnetocaloric properties in $Pr_{0.5}Eu_{0.1}Sr_{0.4}MnO_3$ manganites, Journal of Alloys and Compounds 626 (2015) 20–28.

[41] M. D. Daivajna, A. Rao, Magnetocaloric effect in pristine and Bi-doped $Pr_{0.6}Sr_{0.4}MnO_3$ manganite, Solid State Communications 245 (2016) 65–69.

[42] D. Szewczyk, R. Thaljaoui, J. Mucha, P. Stachowiak, P. Vanderbemden, Specific heat and magnetocaloric effect in $Pr_{0.6}Sr_{0.4-x}Ag_xMnO_3$ manganites, Intermetallics 102 (2018) 88–93.

[43] A. Gamzatov, A. Aliev, P. Yen, L. Khanov, K. Hau, T. Thanh, N. Dung, S.-C. Yu, Correlation of the magnetocaloric effect and magnetostriction near the first-order phase transition in $Pr_{0.7}Sr_{0.2}Ca_{0.1}MnO_3$ manganite, Journal of Applied Physics 124 (18) (2018) 183902.

[44] A. Batdalov, A. Gamzatov, A. Aliev, N. Abdulkadirova, P. Yen, T. Thanh, N. Dung, S.-C. Yu, Magnetocaloric properties in the $Pr_{0.7}Sr_{0.3-x}Ca_xMnO_3$: Direct and indirect estimations from thermal diffusivity data, Journal of Alloys and Compounds 782 (2019) 729–734.

[45] A. Nasri, E. Hlil, A.-F. Lehlooh, M. Ellouze, F. Elhalouani, Study of magnetic transition and magnetic entropy changes of $Pr_{0.6}Sr_{0.4}MnO_3$ and $Pr_{0.6}Sr_{0.4}Mn_{0.9}Fe_{0.1}O_3$ compounds, The European Physical Journal Plus 131 (4) (2016) 1–6.

[46] A. Gamzatov, A. Batdalov, A. Aliev, Z. Khurshilova, M. Ellouze, F. B. Jemma, Specific heat, thermal diffusion, thermal conductivity and magnetocaloric effect in $Pr_{0.6}Sr_{0.4}Mn_{1-x}Fe_xO_3$ manganites, Journal of Magnetism and Magnetic Materials 443 (2017) 352–357.

[47] A. Gamzatov, A. Batdalov, A. Aliev, M. Ellouze, F. Jemma, Heat capacity and the magnetocaloric effect in $Pr_{0.6}Sr_{0.4}Mn_{1-x}Fe_xO_3$ manganite, Physics of the Solid State 59 (10) (2017) 2092–2096.

[48] K. Snini, F. B. Jemaa, M. Ellouze, E. Hlil, Structural, magnetic and magnetocaloric investigations in $Pr_{0.67}Ba_{0.22}Sr_{0.11}Mn_{1-x}Fe_xO_3$ ($0 \leq x \leq 0.15$) manganite oxide, Journal of Alloys and Compounds 739 (2018) 948–954.

[49] V. Markovich, I. Fita, R. Puzniak, A. Wisniewski, K. Suzuki, J. Cochrane, Y. Yuzhelevskii, Y. M. Mukovskii, G. Gorodetsky, Pressure effects on the magnetic and transport properties of $Pr_{1-x}Sr_xMnO_3$ crystals near the percolation threshold, Physical Review B 71 (22) (2005) 224409.

[50] V. Markovich, I. Fita, R. Puzniak, C. Martin, A. Wisniewski, C. Yaicle, A. Maignan, G. Gorodetsky, Pressure effect on magnetism in phase-separated Cr-doped $Pr_{0.5}Ca_{0.5}Mn_{1-x}Cr_xO_3$ manganites, Journal of Magnetism and Magnetic Materials 316 (2) (2007) e636–e639.

[51] R. Thiyagarajan, S. Esakki Muthu, S. Barik, R. Mahendiran, S. Arumugam, Effect of hydrostatic pressure on magnetic entropy change and critical behavior of the perovskite manganite $La_{0.4}Bi_{0.3}Sr_{0.3}MnO_3$, Journal of Applied Physics 113 (2) (2013) 023904.

[52] H. B. Khlifa, Y. Regaieg, W. Cheikhrouhou-Koubaa, M. Koubaa, A. Cheikhrouhou, Structural, magnetic and magnetocaloric properties of K-doped $Pr_{0.8}Na_{0.2-x}K_xMnO_3$ manganites, Journal of Alloys and Compounds 650 (2015) 676–683.

[53] B. Arun, V. Akshay, G. R. Mutta, C. Venkatesh, M. Vasundhara, Mixed rare earth oxides derived from monazite sand as an inexpensive precursor material for room temperature magnetic refrigeration applications, Materials Research Bulletin 94 (2017) 537–543.

[54] S. K. Vandrangi, J.-C. Yang, Y.-M. Zhu, Y.-Y. Chin, H.-J. Lin, C.-T. Chen, Q. Zhan, Q. He, Y.-C. Chen, Y.-H. Chu, Enhanced magnetocaloric effect driven by interfacial magnetic coupling in self-assembled $Mn_3O_4 - La_{0.7}Sr_{0.3}MnO_3$ nanocomposites, ACS applied materials & interfaces 7 (48) (2015) 26504–26511.

[55] A. Marzouki-Ajmi, W. Cheikrouhou-Koubaa, A. Cheikhrouhou,

Magnetic and magnetocaloric study of polycrystalline (1-x)$La_{0.65}Ca_{0.35}MnO_3$/xFe_2O_3 composites, Journal of Superconductivity and Novel Magnetism 28 (1) (2015) 103–108.

[56] S. Vadnala, P. Pal, S. Asthana, Investigation of near room temperature magnetocaloric, magnetoresistance and bolometric properties of $Nd_{0.5}La_{0.2}Sr_{0.3}MnO_3$: Ag_2O manganites, Journal of Materials Science: Materials in Electronics 27 (6) (2016) 6156–6165.

[57] M. Nasri, J. Khelifi, M. Triki, E. Dhahri, E. Hlil, Impact of CuO phase on magnetocaloric and magnetotransport properties of $La_{0.6}Ca_{0.4}MnO_3$ ceramic composites, Journal of Alloys and Compounds 678 (2016) 427–433.

[58] A. E.-M. A. Mohamed, V. Vega, M. Ipatov, A. Ahmed, B. Hernando, Annealing temperature effect on magnetic and magnetocaloric properties of manganites, Journal of Alloys and Compounds 665 (2016) 394–403.

[59] A. E.-M. A. Mohamed, M. A. Mohamed, V. Vega, B. Hernando, A. Ahmed, Tuning magnetoresistive and magnetocaloric properties via grain boundaries engineering in granular manganites, RSC Advances 6 (81) (2016) 77284–77290.

[60] T. Gavrilova, I. Gilmutdinov, J. Deeva, T. Chupakhina, N. Lyadov, I. Faizrakhmanov, F. Milovich, Y. V. Kabirov, R. Eremina, Magnetic and magnetocaloric properties of (1-x)$La_{0.7}Sr_{0.3}MnO_3$/xNaF composites, Journal of Magnetism and Magnetic Materials 467 (2018) 49–57.

[61] N. Amri, M. Nasri, M. Triki, E. Dhahri, Synthesis and characterization of (1 x)($La_{0.6}Ca_{0.4}MnO_3$)/x(Sb_2O_3) ceramic composites, Phase Transitions 92 (1) (2019) 52–64.

[62] R. N. Mahato, K. Sethupathi, V. Sankaranarayanan, R. Nirmala, Large magnetic entropy change in nanocrystalline $Pr_{0.7}Sr_{0.3}MnO_3$, Journal of Applied Physics 107 (9) (2010) 09A943.

[63] S. Ng, K. Lim, S. Halim, H. Jumiah, Grain size effect on the electrical and magneto-transport properties of nanosized $Pr_{0.67}Sr_{0.33}MnO_3$, Results in Physics 9 (2018) 1192–1200.

[64] A. D. Souza, M. Vagadia, M. Daivajna, Effect of nanoscale size reduction on the magnetic properties of $Pr_{0.6}Sr_{0.4}MnO_3$, Journal of Magnetism and Magnetic Materials 538 (2021) 168280.

[65] H. Bouhani, A. Endichi, D. Kumar, O. Copie, H. Zaari, A. David, A. Fouchet, W. Prellier, O. Mounkachi, M. Balli, et al., Engineering the magnetocaloric properties of $PrVO_3$ epitaxial oxide thin films by strain effects, Applied Physics Letters 117 (7) (2020) 072402.

[66] M. Fan, H. Wang, S. Misra, B. Zhang, Z. Qi, X. Sun, J. Huang, H. Wang, Microstructure, magnetic, and magnetoresistance properties of $La_{0.7}Sr_{0.3}MnO_3$: CuO nanocomposite thin films, ACS applied materials & interfaces 10 (6) (2018) 5779–5784.

[67] Q. Chen, Y. Yang, Y. Gao, R. Xu, H. Zhang, J. Ma, et al., Silver addition in polycrystalline $La_{0.7}Ca_{0.3}MnO_3$: Large magnetoresistance and anisotropic magnetoresistance for manganite sensors, Journal of Alloys and Compounds (2021) 160719.

[68] H. D. Shah, J. Bhalodia, Electrical, magnetotransport and magnetization studies of (1-x)$La_{0.7}Sr_{0.3}Mn_{0.94}Co_{0.06}O_3$/xZnO (x= 0, 0.04) composite, Cryogenics 114 (2021) 103244.

[69] B.-x. Huang, Y.-h. Liu, R.-z. Zhang, C.-j. Wang, L.-m. Mei, et al., Low-field MR behaviour in $La_{0.67}Ca_{0.33}MnO_3/ZrO_2$ composite system, Journal of Physics D: Applied Physics 36 (16) (2003) 1923.

[70] S. Karmakar, S. Taran, B. Chaudhuri, H. Sakata, C. Sun, C. Huang, H. Yang, Study of grain boundary contribution and enhancement of magnetoresistance in $La_{0.67}Ca_{0.33}MnO_3/V_2O_5$ composites, Journal of Physics D: Applied Physics 38 (20) (2005) 3757.

[71] H. Yang, Z. Cao, X. Shen, T. Xian, W. Feng, J. Jiang, Y. Feng, Z. Wei, J. Dai, Fabrication of 0-3 type manganite/insulator composites and manipulation of their magnetotransport properties, Journal of Applied Physics 106 (10) (2009) 104317.

[72] X. Gao, L. Li, J. Jian, J. Huang, X. Sun, D. Zhang, H. Wang, Tunable low-field magnetoresistance properties in $(La_{0.7}Ca_{0.3}MnO_3)_{1-x}$: $(CeO_2)_x$ vertically aligned nanocomposite thin films, Applied Physics Letters 115 (5) (2019) 053103.

[73] K. El Maalam, M. Balli, S. Habouti, M. Dietze, M. Hamedoun, E.-K. Hlil, M. Es-Souni, A. El Kenz, A. Benyoussef, O. Mounkachi, Composite ($La_{0.45}Nd_{0.25}$)$Sr_{0.3}MnO_3$/5CuO materials for magnetic refrigeration applications, Journal of Magnetism and Magnetic Materials 449 (2018) 25–32.

[74] R. C. Bhatt, V. Awana, H. Kishan, P. Srivastava, Near room temperature magneto-transport (TCR & MR) and magnetocaloric effect in $Pr_{2/3}Sr_{1/3}MnO_3$: Ag_2O composite, Journal of Alloys and Compounds 619 (2015) 151–156.

[75] D. Neupane, L. Hulsebosch, A. K. Pathak, S. R. Mishra, Magnetocaloric study of $La_{0.45}Nd_{0.25}Sr_{0.3}MnO_3$/MO (MO= CuO, CoO, and NiO) nanocomposites., IEEE Transactions on Magnetics (2021).

[76] M.-H. Phan, H.-X. Peng, S.-C. Yu, Large magnetocaloric effect in single crystal $Pr_{0.63}Sr_{0.37}MnO_3$, Journal of applied physics 97 (10) (2005) 10M306.

[77] V. Markovich, A. Wisniewski, H. Szymczak, Magnetic properties of perovskite manganites and their modifications, in: Handbook of Magnetic Materials, Vol. 22, Elsevier, 2014, pp. 1–201.

[78] M. Shaikh, D. Varshney, Structural and electrical properties of $Pr_{1-x}Sr_xMnO_3$ (x= 0.25, 0.3, 0.35 and 0.4) manganites, Materials science in semiconductor processing 27 (2014) 418–426.

[79] A. K. Saw, G. Channagoudra, S. Hunagund, R. L. Hadimani, V. Dayal, Study of transport, magnetic and magnetocaloric properties in Sr^{2+} substituted praseodymium manganite, Materials Research Express 7 (1) (2020) 016105.

[80] D. Maheswar Repaka, T. Tripathi, M. Aparnadevi, R. Mahendiran, Magnetocaloric effect and magnetothermopower in the room temperature ferromagnet $Pr_{0.6}Sr_{0.4}MnO_3$, Journal of Applied Physics 112 (12) (2012) 123915.

[81] A. Chanda, R. Mahendiran, Effects of external magnetic field and hydrostatic pressure on magnetic and structural phase transitions in $Pr_{0.6}Sr_{0.4}MnO_3$, Journal of Applied Physics 124 (4) (2018) 043902.

[82] O. Chdil, M. Balli, P. De Rango, K. El Maalam, A. El Boukili, O. Mounkachi, Assessment of near $Pr_{2/3}Sr_{1/3}MnO_3$ oxide in magnetic cooling, International Journal of Refrigeration 133 (2022) 302–312.

[83] Z.-Y. Zhou, X.-S. Wu, G.-S. Luo, F.-Y. Jiang, Effect of second introduced phase on magnetotransport properties of $La_{2/3}Sr_{1/3}MnO_3$/0.33 (CuO, ZnO, Al_2O_3) composites, Transactions of Nonferrous Metals Society of China 18 (4) (2008) 890–896.

[84] C. Díaz-Guerra, M. Vila, J. Piqueras, Exchange bias in single-crystalline CuO nanowires, Applied Physics Letters 96 (19) (2010) 193105.

[85] W. Siemons, G. Koster, D. H. Blank, R. H. Hammond, T. H. Geballe, M. R. Beasley, Tetragonal CuO: End member of the 3d transition metal monoxides, Physical Review B 79 (19) (2009) 195122.

[86] T. Degen, M. Sadki, E. Bron, U. König, G. Nénert, The highscore suite, Powder Diffraction 29 (S2) (2014) S13–S18.

[87] T. Roisnel, J. Rodriguez-Carvajal, Computer program fullprof, LLB-LCSIM, May (2003).

[88] B. H. Toby, R factors in rietveld analysis: How good is good enough?, Powder diffraction 21 (1) (2006) 67–70.

[89] J. Alonso, M. Martinez-Lope, M. Casais, M. Fernandez-Diaz, Evolution of the jahn- teller distortion of mno6 octahedra in $RMnO_3$ perovskites (R= Pr, Nd, Dy, Tb, Ho, Er, Y): a neutron diffraction study, Inorganic chemistry 39 (5) (2000) 917–923.

[90] P. Radaelli, G. Iannone, M. Marezio, H. Hwang, S. Cheong, J. Jorgensen, D. Argyriou, Structural effects on the magnetic and transport properties of perovskite $A_{1-x}A'_xMnO_3$ (x= 0.25, 0.30), Physical Review B 56 (13) (1997) 8265.

[91] Y. Tokura, Critical features of colossal magnetoresistive manganites, Reports on Progress in Physics 69 (3) (2006) 797.

[92] Y.-C. Liou, C.-T. Wu, Y.-L. Huang, T.-C. Chung, Effect of CuO on $CaTiO_3$ perovskite ceramics prepared using a direct sintering process, Journal of nuclear materials 393 (3) (2009) 492–496.

[93] W. Mabrouki, A. Krichene, N. Chniba Boudjada, W. Boujelben, Sintering temperature effect on the magnetic properties of $Pr_{0.67}Sr_{0.33}MnO_3$ manganite, Applied Physics A 126 (3) (2020) 1–12.

[94] L. Xu, J. Fan, Y. Zhu, Y. Shi, L. Zhang, L. Pi, Y. Zhang, D. Shi, Magnetocaloric effect and spontaneous magnetization in perovskite manganite $Nd_{0.55}Sr_{0.45}MnO_3$, Materials Research Bulletin 73 (2016) 187–191.

[95] B. Martinez, V. Laukhin, J. Fontcuberta, L. Pinsard, A. Revcolevschi, Magnetic field and pressure effects on the magnetic transitions of $La_{0.9}Ca_{0.1}MnO_3$ perovskites, Physical Review B 66 (5) (2002) 054436.

[96] B. Banerjee, On a generalised approach to first and second order magnetic transitions, Physics letters 12 (1) (1964) 16–17.

[97] X. Moya, S. Kar-Narayan, N. D. Mathur, Caloric materials near ferroic phase transitions, Nature materials 13 (5) (2014) 439–450.

[98] M. Balli, D. Fruchart, D. Gignoux, R. Zach, The "colossal" magnetocaloric effect in $Mn_{1-x}Fe_xAs$: What are we really measuring?, Ap-

plied Physics Letters 95 (7) (2009) 072509.
[99] J. Mira, J. Rivas, L. Hueso, F. Rivadulla, M. Lopez Quintela, Drop of magnetocaloric effect related to the change from first-to second-order magnetic phase transition in $La_{2/3}(Ca_{1-x}Sr_x)_{1/3}MnO_3$, Journal of Applied Physics 91 (10) (2002) 8903–8905.
[100] K. Gschneidner Jr, V. K. Pecharsky, Magnetocaloric materials, Annual Review of Materials Science 30 (1) (2000) 387–429.
[101] P. Radaelli, D. Cox, M. Marezio, S.-W. Cheong, P. Schiffer, A. Ramirez, Simultaneous structural, magnetic, and electronic transitions in $La_{1-x}Ca_xMnO_3$ with $x = 0.25$ and 0.50, Physical review letters 75 (24) (1995) 4488.
[102] J. B. Goodenough, Theory of the role of covalence in the perovskite-type manganites [La,M(II)]MnO_3, Physical Review 100 (2) (1955) 564.
[103] E. Dagotto, T. Hotta, A. Moreo, Colossal magnetoresistant materials: the key role of phase separation, Physics reports 344 (1-3) (2001) 1–153.
[104] M. B. Salamon, M. Jaime, The physics of manganites: Structure and transport, Reviews of Modern Physics 73 (3) (2001) 583.
[105] Y. Lee, S. Park, Y. Hyun, J. Kim, V. Prokhorov, V. Komashko, V. Svetchnikov, Microstructural and magnetotransport properties of $La_{0.7}Ca_{0.3}MnO_3/BaTiO_3$ and $La_{0.7}Sr_{0.3}MnO_3/BaTiO_3$ bilayered films, Physical Review B 73 (22) (2006) 224413.
[106] P. Dey, T. Nath, Effect of grain size modulation on the magneto-and electronic-transport properties of $La_{0.7}Ca_{0.3}MnO_3$ nanoparticles: The role of spin-polarized tunneling at the enhanced grain surface, Physical Review B 73 (21) (2006) 214425.
[107] J.-H. Park, E. Vescovo, H.-J. Kim, C. Kwon, R. Ramesh, T. Venkatesan, Magnetic properties at surface boundary of a half-metallic ferromagnet $La_{0.7}Sr_{0.3}MnO_3$, Physical review letters 81 (9) (1998) 1953.
[108] M. Balli, D. Fruchart, D. Gignoux, Optimization of $La(Fe,Co)_{13-x}Si_x$ based compounds for magnetic refrigeration, Journal of Physics: Condensed Matter 19 (23) (2007) 236230.
[109] M. Balli, D. Fruchart, D. Gignoux, The $LaFe_{11.2}Co_{0.7}Si_{1.1}C_x$ carbides for magnetic refrigeration close to room temperature, Applied Physics Letters 92 (23) (2008) 232505.
[110] L. Yuan, S. Qian, J. Yu, Numerical study on the multi-layered magnetocaloric regenerators, Applied Thermal Engineering 204 (2022) 118001.
[111] A. Smaıli, R. Chahine, Composite materials for ericsson-like magnetic refrigeration cycle, Journal of applied physics 81 (2) (1997) 824–829.
[112] M. Balli, D. Fruchart, D. Gignoux, E. Hlil, S. Miraglia, P. Wolfers, Gd1-xtbx alloys for ericsson-like magnetic refrigeration cycles, Journal of alloys and compounds 442 (1-2) (2007) 129–131.
[113] G. Diguet, G. Lin, J. Chen, Performance characteristics of a regeneration ericsson refrigeration cycle using a magnetic composite as the working substance, international journal of refrigeration 36 (3) (2013) 958–964.
[114] Z. Xu, G. Lin, J. Chen, A Gd_xHo_{1-x}-based composite and its performance characteristics in a regenerative ericsson refrigeration cycle, Journal of Alloys and Compounds 639 (2015) 520–525.
[115] A. Smaıli, R. Chahine, Thermodynamic investigations of optimum active magnetic regenerators, Cryogenics 38 (2) (1998) 247–252.